IOP Conference Series:
Earth and
Environmental Science

PAPER • **OPEN ACCESS**

Velocity profiles in a water jet of a Pelton nozzle: CFD simulations on both 2D and 3D geometries

To cite this article: D. Stivala *et al* 2021 *IOP Conf. Ser.: Earth Environ. Sci.* **774** 012106

IOP Conf. Series: Earth and Environmental Science **774** (2021) 012106 doi:10.1088/1755-1315/774/1/012106

Velocity profiles in a water jet of a Pelton nozzle: CFD simulations on both 2D and 3D geometries

D. Stivala[1], **M. Rossi**[1], **M. Renzi**[1]

[1] Free University of Bozen-Bolzano, Faculty of Science and Technology, Piazza Università 5, 39100, Bolzano (BZ), Italy

E-mail: massimiliano.renzi@unibz.it

Abstract. Hydropower is an important energy sector deployed all over the World with a significant share in the global electricity production. Due to the ongoing climate changes, the lack of water in summer periods compromises the performance of hydraulic machines, whose efficiency quickly decreases when they operate at strong part-load conditions.

Among the most known hydraulic turbines, Pelton is suitable to be used with high geodetic heights and relatively low flow rates. When dealing with flow rates 30% lower than the Best Efficiency Point (BEP), the efficiency drastically decreases mainly due to the non-uniform velocity profiles of the water jets coming out from the nozzles. The quality of the jet is affected by the distributor geometry, bending pipes and spear valves with the respective supports located upstream.

The aim of this work is to investigate different velocity profiles of the water jet coming out from a Pelton nozzle geometry by means of Computational Fluid Dynamics (CFD) simulations performed by ANSYS® Fluent solver. Four different spear valve angles were simulated on a 2D-axisymmetric geometry, starting from a reference case of $\beta = 50°$ with increasing steps of 5°, maintaining a fixed positioning of the spear valve that corresponds to a partial load operation of the machine.

In addition, also a 3D simulation has been carried out and the streamlines along a symmetry plane are shown. The results of the 3D simulations were compared to the 2D-axisymmetric ones taking into account the aforementioned reference case, showing how this last simplification of the computational domain leads to almost the same macroscopic results.

1. Introduction

The renewable energy sector is becoming more and more important in the global energy scenario for the electricity production: for instance, it contributed to the global electricity demand with a share of around 24.5% by the end of 2016, as reported in the 2017 Edition of the REN21 Renewables Global Status Report [1].

In particular, hydropower plays a key role since it supplied 16.6% of the total global electricity production in the year 2016. However, the growth of the hydropower sector has seen a significant reduction in the last few years since most of the water sources

have been already exploited so far, even though few places in Asia, where dams can be built, still remain available [2].

Hydraulic turbines, such as Pelton [3, 4], Francis [5, 6] and Kaplan [7, 8] ones, are designed according to the design data, in terms of flow rate and head, of the installation site and their development has faced an important boost mainly due to the use of Computational Fluid Dynamic (CFD) tools.

Focusing the attention on the Pelton wheel, this hydraulic machine is an action turbine and it is characterized by low values of specific speed since exploits low flow rates and high heads. The water arrives inside the nozzles through a distributor, which splits the water flow according to the number of nozzles. Then, the water impinges on buckets located on the wheel periphery. Each nozzle has a spear valve that can slide axially to regulate the flow rate exiting from the nozzle, thus providing the water with the best momentum exchange when it impinges on the buckets.

Due to the effects of climate changes, in summer periods the lack of water compromises the performance of a Pelton turbine since the efficiency quickly decreases when operating at strong part-load conditions. Several studies have been performed so far on the Pelton nozzle design to study secondary flows and improve the water jet quality. Chongki et al. [9] carried out numerical simulations on a 3D Pelton nozzle with a bend upstream by investigating the external flow field when three different spear strokes are used. Results showed a higher dispersion of the water jet when the nozzle opening is increased, thus leading to higher hydraulic losses and poor performance of the Pelton bucket. Zhang et al. [10] performed CFD simulations on a 3D Pelton nozzle where a spear angle of 70° was used, achieving higher values of efficiency compared to the standard one of 50°. Along the same line, Petley et al. [11] studied both experimentally and numerically how the nozzle and the spear valve configuration affect the performance of a Pelton turbine. Even if it was identified that injectors with notably steeper nozzle and spear angles achieve higher performance than the standard ones, experimental evidence suggested that a upper limit exists beyond which steeper angles designs are no longer optimal. Kumashiro et al. [12] focused the attention on unsteady flow patterns around the bucket, which depend on the water jet non-uniformity due to the secondary flows created mainly by distributor, bending pipes and spear valves together with respective supports upstream. Both experimental tests and numerical CFD simulations have been performed to validate the numerical results.

The aim of this work is indeed to study different velocity profiles of the water jet coming out from a specific Pelton nozzle geometry with the help of Computational Fluid Dynamics (CFD) analysis through ANSYS® Fluent solver. Four different spear valve angles were simulated on a 2D-axisymmetric geometry, including a reference case of $\beta = 50°$, with increasing steps of 5° maintaining the stroke fixed at $a = 0.5$, which corresponds to a partial load operation of the machine. Indeed, these operating conditions are the most critical and can determine a strong efficiency loss with respect to the nominal one. Regarding the 3D geometry, only the reference case was simulated and macroscopic results, such as mass flow rate $[kg/s]$, maximum axial velocity $[m/s]$ and

average inlet velocity $[m/s]$, were compared to those obtained with the 2D-axisymmetric CFD simulation to understand if a simplified 2D solution can effectively be sufficient to assess the flow field of the water jet.

2. Geometry and mesh

The effects of two main geometrical parameters were investigated in the numerical simulations: i) the axial position of the spear valve and ii) its opening angle. When dealing with the first parameter, a dimensionless number was defined through Eq. (1)

$$a = \frac{l}{d_0} \tag{1}$$

where l is the axial distance of the spear valve from the outlet section of the nozzle and d_0 is the outlet diameter of the nozzle that, in the analysed case, is equal to 36 mm.

The computational domains were extended by almost six times the dimension of the outlet diameter along the axial direction of the nozzle. Furthermore, they were also enlarged to avoid possible recirculating zones of the air. Figures 1 and 2 show the 2D-axisymmetric and the 3D computational domains with $a = 0.5$ and $\beta = 50°$, which constitutes the reference case. Note that the 2D-asymmetric and 3D computational domains correspond to a quarter and half geometry of the Pelton nozzle, respectively, due to XY (2D and 3D) and XZ (2D) symmetry planes that cut down the Pelton nozzle.

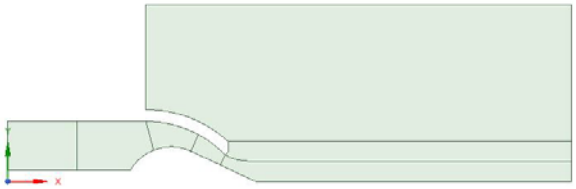

Figure 1. Lateral view of the 2D-axisymmetric nozzle geometry (reference case)

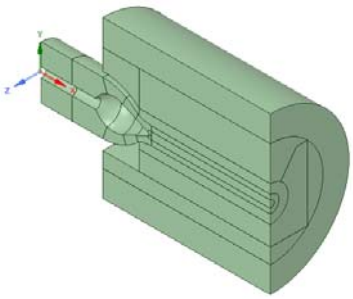

Figure 2. Isometric view of the 3D nozzle geometry (reference case)

Hybrid meshes were generated in both 2D-asymmetric and 3D computational domains. An unstructured mesh close to the location of the air-water interface and a

structured one straight from the outlet of the nozzle until the end of the computational domain were used. In the case of a 2D-axisymmetric grid, mainly quads and triangles elements were employed, while the use of hexahedrals, tetrahedrons, wedges and pyramids was adopted in the 3D one. The zones close to the air-water interface were discretized with a finer mesh as shown in Figures 3 and 4 for both 2D-axisymmetric and 3D geometries, respectively.

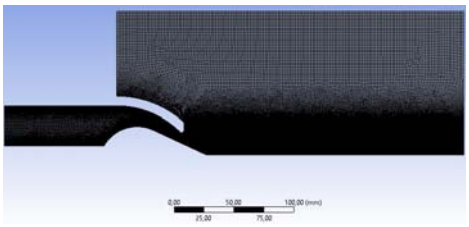

Figure 3. Lateral view of the 2D-axisymmetric nozzle mesh (reference case)

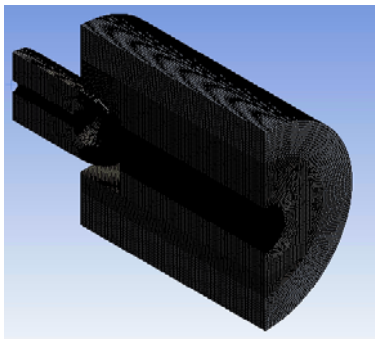

Figure 4. Isometric view of the 3D nozzle mesh (reference case)

It is worth noticing that a further mesh refinement was also performed near the Pelton nozzle and spear walls of the 2D-axisymmetric grid to have an appropriate resolution of the boundary layer and to obtain y^+ values close to 1, which allows to avoid using wall functions. Regarding the 3D grid, in order to limit the computational burden, a maximum value of y^+ equal to 146 was reached close to the spear tip, thus being between $30-300$ as suggested for CFD simulations that deal with turbomachinery applications when wall functions are employed.

To obtain numerical results that are not affected by the mesh pattern and the number of elements, a grid independence study was performed. In this regard, the maximum axial velocity inside the water jet was recorded at a distance equal to 5.5 times the outlet diameter from the nozzle outlet and this value was used as reference to compare the CFD results obtained using different grid densities. In particular, three different grids were generated where GRID 1 and GRID 2 have a number of elements that are approximately 25-30% and 50-60% higher than that of GRID 0, respectively. To assess the obtained results, the absolute relative percentage differences (*arpd*) of the

maximum axial velocities (v) obtained with the previous three grids were evaluated by Eq. 2.

$$arpd\,(\%) = \frac{v_{GRIDn+1} - v_{GRIDn}}{v_{GRIDn}} \cdot 100 \tag{2}$$

Since the absolute relative percentage difference of the maximum axial velocity values belonging to two continuous meshes was lower than 1%, the mesh independence study of the 2D-axisymmetric geometry was fulfilled. Table 1 lists the number of elements and the absolute relative percentage differences of the maximum axial velocities measured inside the water jet, which were recorded at the section previously defined.

Table 1. Results of the 2D-axisymmetric mesh independence study

Type of grid	**Number of elements**	**arpd** [%]
GRID 0	87,523	0
GRID 1	102,578	-0.424%
GRID 2	130,421	-0.086%

Even though the absolute relative percentage difference of the axial velocities in GRID 1 and GRID 2 was significantly smaller than 1% with respect to GRID 0, GRID 1 was selected due to a better decrease of the residuals trend. The 3D mesh was similarly studied but with only two different grids. Table 2 lists the number of elements and the absolute relative percentage differences of the maximum axial velocities measured inside the water jet, recorded at the section previously defined.

Table 2. Results of the 3D mesh independence study

Type of grid	**Number of elements**	**arpd** [%]
GRID 0	1,767,050	0
GRID 1	2,118,152	-0.025%

Since the absolute relative percentage difference of the maximum axial velocity values belonging to two continuous meshes was strongly lower than 1%, the mesh independence study 3D geometry was fulfilled and thus GRID 0 was selected.

3. Numerical setup

Steady-state simulations were performed using the Volume-Of-Fluids (VOF) model with two Eulerian phases active, as well as the coupled level set+VOF option, to study this multiphase problem. It is worth noticing that the pseudo-transient option was enabled, allowing the simulated case to be stable and, at the same time, achieve a faster convergence.

Physical characteristics of both air and water were imported from ANSYS® Fluent library. Air was selected as primary phase, while water as secondary one. The value of

the surface tension between air and water was kept constant and equal to 0.072 N/m, which corresponds to the value at standard operating conditions.

The $k-\omega$ Shear Stress Transport (SST) and the realizable $k-\epsilon$ turbulence models were used in the 2D-axisymmetric and 3D geometries, respectively.

The inlet section of the Pelton nozzle was filled by water and a relative static pressure-inlet BC of 1.5 *bar* was set with the default turbulence intensity values. The no-slip option and default values of roughness were retained for both nozzle and spear valve walls. A relative static pressure of 0 *bar* was set along the boundaries of the computational domains where the air is present at time zero, maintaining also default backflow values. The operating pressure was set equal to 1 *bar* and the specified operating density was enabled and retained equal to the air one, which is equal to 1.225 kg/m^3. This excludes the buildup of hydrostatic pressure within the lighter phase, improving the round-off accuracy for the momentum balance.

Table 3 lists the main algorithms/schemes used to perform CFD simulations on both 2D-axisymmetric and $3D$ computational domains.

Table 3. Algorithms/schemes used in the CFD simulations

Solution methods	**Algorithm/scheme**
Pressure-Velocity Coupling	PISO
Spatial Discretization of Gradient	LSCB
Spatial Discretization of Pressure	PRESTO!
Spatial Discretization of Momentum	Second Order Upwind
Spatial Discretization of Volume fraction	Compressive
Spatial Discretization of Turbulent Kinetic Energy	Second Order Upwind
Spatial Discretization of Turbulent Dissipation Rate	Second Order Upwind

Finally, the convergence was achieved when Root Mean Squares (RMS) residuals variations between successive iterations was lower than 10^{-6} and 10^{-4} for 2D-axisymmetric and 3D simulations, respectively.

4. Numerical simulations

Figure 5 shows three velocity profiles at different water jet sections considering $a = 0.5$ and $\beta = 50°$. The analysed sections are located at $1.44 \cdot d_0$, $2.83 \cdot d_0$ and $4.22 \cdot d_0$ from the outlet section of the Pelton nozzle, respectively. The velocity values close to the axis of symmetry are smaller compared to those in the upper part, as previously stated, due to the influence of the spear valve downstream the nozzle. Moreover, the profile becomes more uniform as the distance from the nozzle increases. Going more into detail, Figures 6, 7, 8 and 9 show the axial velocity profiles obtained in the analysed four cases, where a was kept constant at 0.5. Each plot shows the velocity profiles at the sections previously indicated obtained per each value of β, considering an increasing step of 5 degrees from 50° to 65°. The lengths of 200 mm, 250 mm and 300 mm refer to the distance between

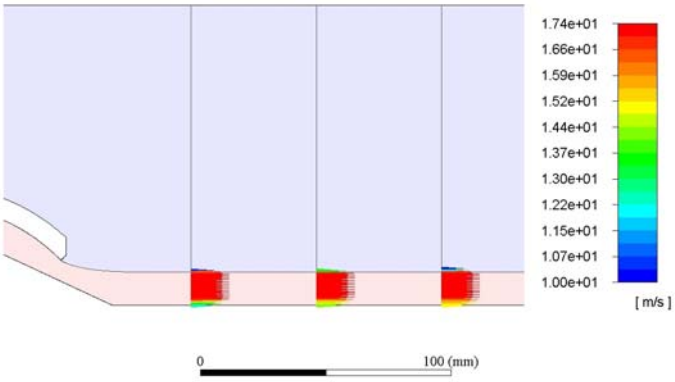

Figure 5. Velocity profiles at $1.44 \cdot d_0$, $2.83 \cdot d_0$ and $4.22 \cdot d_0$ from the outlet section of the nozzle

the inlet section of the nozzle and each analysed section. The case with the largest spear valves angle ($\beta = 65°$) showed the best result considering the uniformity of the velocity profiles, as reported in Figure 9. In this case, the velocity along the axis of symmetry in the first section is already greater than 14 m/s with respect to the one obtained with $\beta = 50°$, where a value close to 12 m/s was obtained as reported in Figure 6. Then, the standard spear angle of $\beta = 50°$ seems to be not optimal for low head operating conditions as in this case since the spear valve affects the flow velocity downstream the nozzle. Finally, analysing the results from Figure 6 to Figure 9, the higher the spear valve angle, the more uniform the velocity profile when the spear valve stroke is fixed, thus suggesting a possible modification of the Pelton nozzle to work in each operating condition properly.

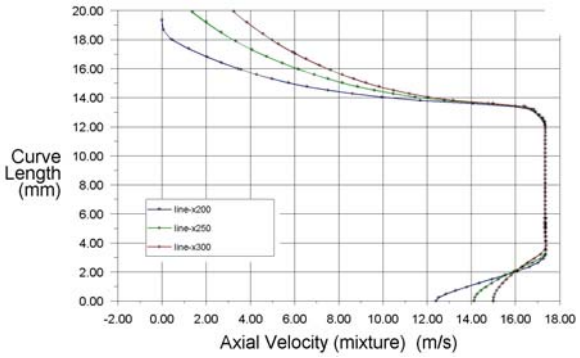

Figure 6. Velocity profiles obtained with the reference case

After the analysis of the CFD simulation related to the 2D-axisymmetric geometry, the comparison of the obtained macroscopic results, such as mass flow rate $[kg/s]$, maximum axial velocity $[m/s]$ and average inlet velocity $[m/s]$, with the ones recorded in the 3D simulations was performed as listed in Table 4. It is worth noticing that the results shown in Table 4 refer to the reference case.

The mass flow rate, as well as the water velocity at the inlet section, resulted to

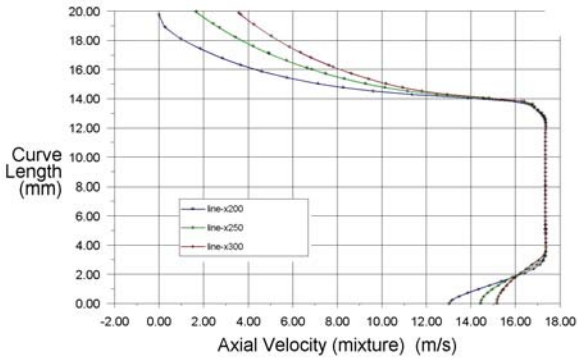

Figure 7. Velocity profiles obtained with $a = 0.5$ and $\beta = 55°$

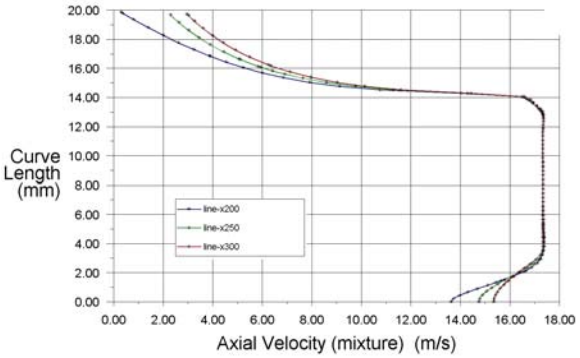

Figure 8. Velocity profiles obtained with $a = 0.5$ and $\beta = 60°$

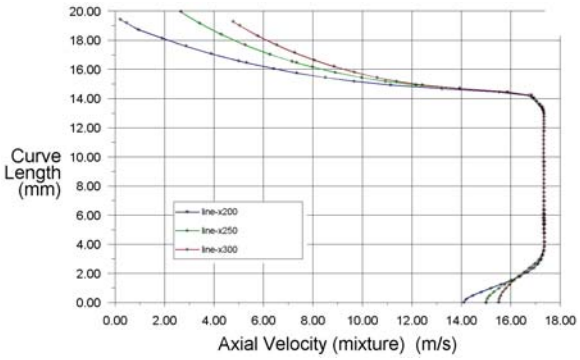

Figure 9. Velocity profiles obtained with $a = 0.5$ and $\beta = 65°$

Table 4. Comparison between 2D-axisymmetric and 3D results

Geom.	**Mass flow rate** $[kg/s]$	**Max. velocity** $[m/s]$	**Average inlet velocity** $[m/s]$
2D	9.46	17.38	1.88
3D	9.58	17.34	1.90

be slightly lower in the 2D-axisymmetric CFD simulation than those in the 3D one, while the maximum axial velocity, which was recorded at a distance from the discharge

section of 4.22 times the outlet diameter d_0, was slightly lower. However, since the maximum absolute difference between 2D-axisymmetric and 3D CFD simulations was equal to 1.3% (mass flow rate), no substantial differences were noticed, meaning that the 2D-axisymmetric geometry is appropriate for their evaluation. In any case, 3D CFD simulations become of interest when particular detail of the air-water interactions have to be studied. Finally, Figure 10 shows the pathlines of the water jet coloured by velocity magnitude to have an overview of the possible flow path in a 3D nozzle.

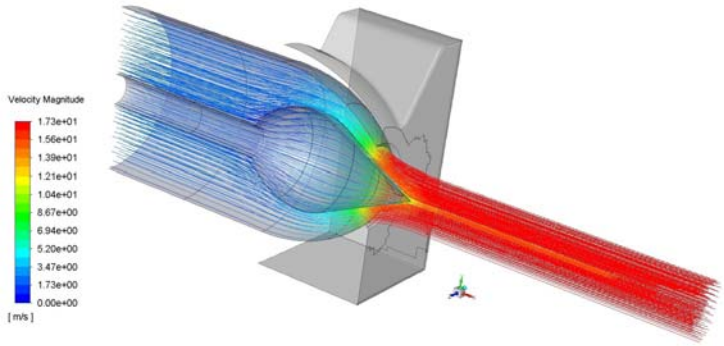

Figure 10. 3D flow pathlines coloured by velocity magnitude

5. Conclusions

Velocity profiles of the water jet coming out from a specific Pelton nozzle geometry were studied by means of Computational Fluid Dynamics (CFD) simulations performed by ANSYS® Fluent solver.

The problem was studied using a 2D-axisymmetric geometry, where both XY and XZ symmetry planes cut down a quarter of the Pelton nozzle. In addition, a CFD simulation on a 3D geometry, where a XY symmetry plane cut down half of the Pelton nozzle, was also performed considering only the reference case of $a = 0.5$ and $\beta = 50°$.

The 2D-axisymmetric mesh includes a further refinement of the boundary layer since a near wall approach for the turbulence modelling was chosen, while no further refinements were done in the 3D mesh where wall functions were used. Moreover, a mesh independence study was carried out for both geometries.

A Multiphase Volume-Of-Fluids (VOF) model with two Eulerian phases active and the coupled level set+VOF option were selected due to the presence of both air and water. The $k - \omega$ SST turbulence model was chosen for the closure of the Reynolds Averaged Navier-Stokes (RANS) equations in the 2D-asymmetric CFD simulations, while the realizable $k - \epsilon$ was used in the 3D one.

Four different spear valve angles were simulated on a 2D-axisymmetric geometry, starting from the reference case with increasing steps of 5° and maintaining the stroke fixed at $a = 0.5$. Results showed how the velocity profiles downstream the nozzle are affected by the presence of the spear valve. In particular, the case with the largest

spear valves angle ($\beta = 65°$) showed the most uniform velocity profiles analysing three different sections of the water jet, meaning that the higher the spear valve angle, the more uniform the velocity profile at a fixed spear valve stroke.

Finally, macroscopic magnitudes obtained in the 2D-axisymmetric reference case, such as mass flow rate $[kg/s]$, maximum axial velocity $[m/s]$ and average inlet velocity $[m/s]$, were compared to the ones recorded with the 3D geometry. Results showed that the maximum absolute difference between 2D-axisymmetric and 3D CFD simulations was equal to 1.3%, meaning that the 2D-axisymmetric geometry is appropriate for their evaluation. However, 3D CFD simulations are fundamental to study in detail the air-water interactions, such as vortices generations along their interface.

References

[1] REN21 - Renewables 2017 Global Status Report, http://www.ren21.net/gsr-2017
[2] Liu L, Parkinson S, Gidden M, Byers E, Satoh Y, Riahi K and Forman B, Quantifying the potential for reservoirs to secure future surface water yields in the world's largest river basins 2018 *Environ. Res. Lett.* 13 044026 https://doi.org/10.1088/1748-9326/aab2b5
[3] Mack R, Gola B, Smertnig M, Wittwer B and Meusburger P, Modernization of vertical Pelton turbines with the help of CFD and model testing 2014 *IOP Conf. Ser.: Earth Environ. Sci.* 22 012002 https://doi.org/10.1088/1755-1315/22/1/012002
[4] Kholifah N, Setyawan A C, Wijayanto D S, Widiastuti I and Saputro H, Performance of Pelton Turbine for Hydroelectric Generation in Varying Design Parameters 2018 *IOP Conf. Ser.: Mater. Sci. Eng.* 228 012108 https://doi.org/10.1088/1757-899X/288/1/012108
[5] Jakobsen K-R G and Holst M A, CFD simulations of transient load change on a high head Francis turbine 2017 *J. Phys.: Conf. Ser.* 782 012002 https://doi.org/10.1088/1742-6596/782/1/012002
[6] Pochylý F, Rudolf P, Štefan D, Moravec P, Stejskal J and Skoták A, Design of a pump-turbine using a quasi-potential flow approach, mathematical optimization and CFD 2019 *IOP Conf. Ser.: Earth Environ. Sci.* 240 072043 https://doi.org/10.1088/1755-1315/240/7/072043
[7] Motycak L, Skotak A, and Obrovsky J, Analysis of the Kaplan turbine draft tube effect 2010 *IOP Conf. Ser.: Earth Environ. Sci.* 12 012038 https://doi.org/10.1088/1755-1315/12/1/012038
[8] Rivetti A, Lucino C, Liscia S, Muguerza D and Avellan F, CFD simulations of transient load change on a high head Francis turbine 2012 *IOP Conf. Ser.: Earth Environ. Sci.* 15 062035 https://doi.org/10.1088/1755-1315/15/6/062035
[9] Chongji Z, Yexiang X, Wei X, Tao W, Jin Z, Zhengwei W and Yongyao L, Numerical Analysis of Pelton Nozzle Jet Flow Behavior Considering Elbow Pipe 2016 *IOP Conf. Ser.: Earth Environ. Sci.* 49 022005 https://doi.org/10.1088/1755-1315/49/2/022005
[10] Zhang J, Xiao Y X, Wang J Q, Zhou X J, Xia M, Zeng C J, Wang S H and Wang Z W, Optimal design of a pelton turbine nozzle via 3D numerical simulation 2018 *IOP Conf. Ser.: Earth Environ. Sci.* 163 012066 https://doi.org/10.1088/1755-1315/163/1/012066
[11] Petley S, Panagiotopoulos A, Benzon D S, Židonis A, Aggidis G A, Anagnostopoulos J S and Papantonis D E, Investigating the influence of the jet from three nozzle and spear design configurations on Pelton runner performance by numerical simulation 2019 *IOP Conf. Ser.: Earth Environ. Sci.* 240 022004 https://doi.org/10.1088/1755-1315/240/2/022004
[12] Kumashiro T, Alimirzazadeh S, Maertens A, Jahanbakhsh E, Leguizamn S, Avellan F and Tani K, Numerical investigation of the jet velocity profile and its influence on the Pelton turbine performance 2019 *IOP Conf. Ser.: Earth Environ. Sci.* 240 072006 https://doi.org/10.1088/1755-1315/240/7/072006